JOURNAL OF SOLID STATE CHEMISTRY 87, 456–462 (1990)

Phase Diagram of $Cd_{2x}(CuIn)_yMn_{2z}Te_2$ ($x + y + z = 1$) Alloys

MIGUEL QUINTERO, EUNICE GUERRERO, RAFAEL TOVAR, AND G. S. PÉREZ

Centro de Estudios de Semiconductores, Departamento de Física, Universidad de Los Andes, Mérida, Venezuela.

AND JOHN C. WOOLLEY

Ottawa-Carleton Institute for Physics, University of Ottawa, Ottawa, Ontario K1N 6N5, Canada

Received December 18, 1989

The T vs composition phase diagram of the alloy system $Cd_{2x}(CuIn)_yMn_{2z}Te_2$ ($x + y + z = 1$) was investigated in the range $0 < z < 0.80$ by differential thermal analysis and X-ray diffraction measurements. Samples were prepared for various lines of constant x/y ratio and the $T(z)$ data determined for each line. From the values of lattice parameters determined for all samples, the limits of single-phase solid–solution were estimated. In addition to liquidus and solidus curves, the zinc blende–chalcopyrite and Mn-disordered–Mn-ordered transition lines were determined, these phase fields being the ones of interest in the measurements of optical energy gap and magnetic properties.

Introduction

Most of the work (*1, 2*) on semimagnetic semiconductor alloys has been concerned with alloys of the form $II_{1-z}Mn_zVI$. However, similar alloys can be produced from the chalcopyrite I III VI_2 compounds, these being ternary analogs of the II VI compounds. The crystallographic and optical energy gap values of a number of alloy systems of the form $(I\ III)_{1-z}Mn_{2z}Te_2$ have been investigated (*3–7*), and also the work has been extended to the more general $Cd_{2x}(I\ III)_yMn_{2z}Te_2$ ($x + y + z = 1$) alloys (*3, 4*). The magnetic and ESR results for various $(I\ III)_{1-z}Mn_{2z}Te_2$ alloys have been reported (*8, 9*).

These chalcopyrite-based alloys are of interest because, depending upon the heat treatment, the alloys can be produced with the Mn atoms either at random or ordered (or partially ordered) on the cation sublattice. The optical energy gap values and the magnetic behavior are very different in the two different conditions (*7–10*). Before a detailed investigation of the effects of this ordering can be carried out, it is necessary to choose the heat treatment of the alloys so as to produce the required ordered or disordered condition. For this purpose, a detailed knowledge of the T vs composition phase diagram is required. In the present work, the investigation of the Cd-base alloys has been extended to the study of the $T(z)$ diagrams of various sections of the system $Cd_{2x}(CuIn)_yMn_{2z}Te_2$ ($x + y + z = 1$).

0022-4596/90 $3.00

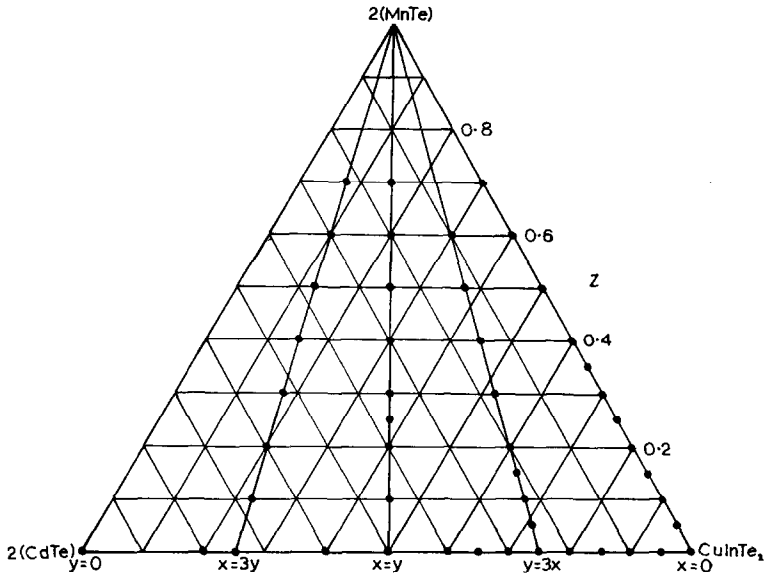

FIG. 1. Composition diagram for the $Cd_{2x}(CuIn)_yMn_{2z}Te_2$ alloys. Composition of alloys used in the present work.

Preparation of Samples and Experimental Measurements

All of the alloys used were produced by the usual melt and anneal technique (*3, 6*). The components of each 1.5-g sample were sealed under vacuum in small quartz ampoules which had previously been carbonized to prevent interaction of the alloy with the quartz, melted together at 1150°C, air cooled to room temperature, and then annealed to equilibrium. As in all such multicomponent alloys, the appropriate temperature of anneal is not easily determined until the T vs composition phase diagram is known for each section. However, the results for the sections $(CuIn)_{1-z}Mn_{2z}Te_2$ and $(AgIn)_{1-z}Mn_{2z}Te_2$ (*6*), already investigated, show that an annealing temperature of 600°C should be satisfactory, and this value was used here. It has been found that at least 20–30 days of annealing is necessary to obtain equilibrium conditions at 600°C, since long-range diffusion may be required after the initial cooling from the melt. Equilibrium at fairly low temperatures is needed if peaks corresponding to order–disorder and chalcopyrite–zinc blende transitions are to be observed in the heating DTA runs. However, once the equilibrium at 600°C has been achieved, zinc blende–chalcopyrite and order–disorder transitions, which involve only short-range diffusion, can occur in much shorter times, even though they occur below 600°C in these systems. In order to produce useful $T(z)$ diagrams, samples were prepared for the sections given by $x = 3y$, $x = y$, $y = 3x$, $x = 0$, and $z = 0$ as shown in Fig. 1. Since the interest of the program is in semimagnetic semiconductors, values of z up to an upper limit of 0.8 only were used, and the Mn-rich phases were not investigated.

X-ray powder photographs, either Guinier or Debye–Scherrer, were used to check the condition of the annealed samples and to determine the phases that were present. Values of lattice parameter were determined

for the zinc blende and chalcopyrite phases, these results having been reported previously (*3*).

Phase transition temperatures were obtained from DTA measurements (*11*), using a closed tube configuration and with silver or gold used as the reference material. The charge was a powdered alloy of approximately 100-mg weight. The temperatures of the sample and of the reference were measured with chromel–alumel thermocouples, the difference signal between sample and reference and also the temperature signal being simultaneously registered on a two-pen chart recorder. Each phase transition temperature was determined from the baseline intercept of the tangent to the leading edge of the peak in the difference signal. Both heating and cooling runs were made for each sample.

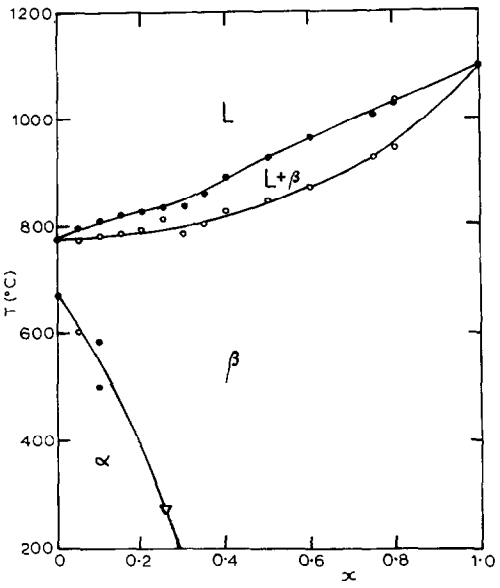

FIG. 2. $T(x)$ diagram for $Cd_{2x}(CuIn)_{1-x}Te_2$ section (i.e., $z = 0$). α is the chalcopyrite and β the zinc blende structure. ○, heating run; ●, cooling run; ▽, from X-ray data.

Results and Discussion

In previous work on the $Cd_{2x}(CuIn)_y Mn_{2z}Te_2$ alloys (*3*), lattice parameter values for samples slowly cooled to room temperature were used to determine the composition ranges of the various single-phase and two-phase fields involving the zinc blende and chalcopyrite phases. With regard to the T vs composition data, the $T(x)$ diagram for the $Cd_{2x}(CuIn)_{1-x}Te_2$ section, i.e., $z = 0$, was given in earlier work (*12*) and that diagram has been repeated here. The diagram of Ref. (*12*) indicates that a narrow ($\alpha + \beta$) two-phase range occurs; this is indicated by dashed lines in Fig. 2 of that paper. However, the values of lattice parameter given (*3, 13*) indicate that, at each value of x in that range, the chalcopyrite and zinc blende phases show the same value of a. As was pointed out in recent work on the lattice parameter values and $T(z)$ diagrams of the $Zn_{2x}(CuIn)_y Mn_{2z}T_2$ alloys (*14, 15*), the various results indicate that the apparent two-phase behavior is due to an order–disorder reaction which is very slow because of the relatively low ordering temperature. Thus the apparent two-phase field represents non-equilibrium conditions. In Fig. 2, the $T(x)$ diagram of this section indicates the estimated boundary between the α and β phases as a single line. Recently the $T(z)$ diagram has been obtained for the $(CuIn)_{1-z}Mn_{2z}Te_2$ section (*5*), i.e., $x = 0$ and for comparison purposes this diagram is shown in Fig. 3. For the case of the $Cd_{1-z}Mn_zTe$ section, i.e., $y = 0$, these data have been given by Triboulet and Didier (*16*).

The $T(z)$ diagrams for the sections $y = 3x$, $x = y$, and $x = 3y$ are shown in Figs. 4, 5, and 6, respectively. In these diagrams, boundaries determined directly from DTA measurements are shown as solid lines. However, some boundaries cannot be determined from the DTA data and these need to be estimated from the lattice parameter and energy gap values determined previously (*3*). These boundaries are shown as

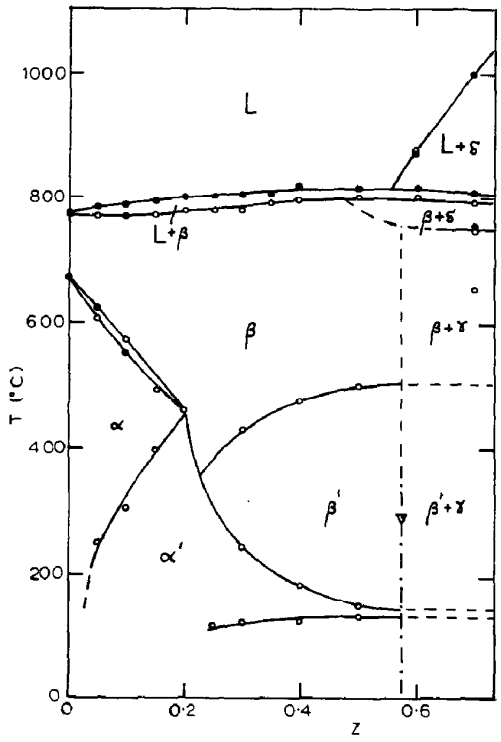

FIG. 3. $T(z)$ diagram for the $(CuIn)_{1-z}Mn_{2z}Te_2$ section (i.e., $x = 0$). α is the Mn-disordered chalcopyrite, α' the Mn-ordered chalcopyrite, β the Mn-disordered zinc blende, β' the Mn-ordered zinc blende, and γ and δ are the NiAs and NaCl structures of MnTe, respectively. ○, heating run; ●, cooling run; ▽, from X-ray data.

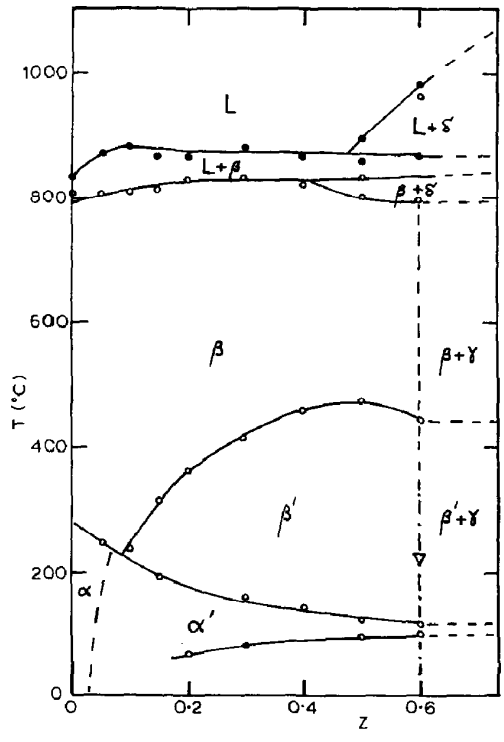

FIG. 4. $T(z)$ diagram for the $y = 3x$ section. α is the Mn-disordered chalcopyrite, α' the Mn-ordered chalcopyrite, β the Mn-disordered zinc blende, β' the Mn-ordered zinc blende, and γ and δ are the NiAs and NaCl structures of MnTe, respectively. ○, heating run; ●, cooling run; ▽, from X-ray data.

dash–dotted lines in the $T(z)$ diagrams, while dashed lines have been used to indicate lines which are estimated only.

As has been shown previously (*17*), Cu $InTe_2$ has the chalcopyrite structure α up to 670°C and then becomes zinc blende β up to its melting point at 770°C. Figures 2, 3, and 4 show that in the sections $z = 0$, $x = 0$, and $y = 3x$ both the α and β phases are present. For the $x = y$ and $x = 3y$ sections (Figs. 5 and 6), the chalcopyrite phase does not occur, but a wide range of zinc blende β phase is observed. With regard to the lower temperature range, i.e., mainly in the range of the single phase solid fields, for the $z = 0$ section (Fig. 2), it is seen that the α phase appears at 672°C for $x = 0$ and that the field achieves a width of approximately $z = 0.25$ at $T = 300$°C. For the higher temperature range of this section, the β phase occurs at all compositions, and for $x > 0.30$ it occurs at all temperatures below the solidus curve. In the $x = 0$ section, the lattice parameter data (*3*) indicate a range of solid solubility in the adamantine phases of $z = 0.59$. For z greater than this, there is two-phase behavior with the γ phase of MnTe with the NiAs structure being observed. As shown in previous work (*6*), the adamantine single phase fields consists of four different ordered structures, α the Mn-disordered chalcopyrite (dc), α' the Mn-ordered chalcopyrite

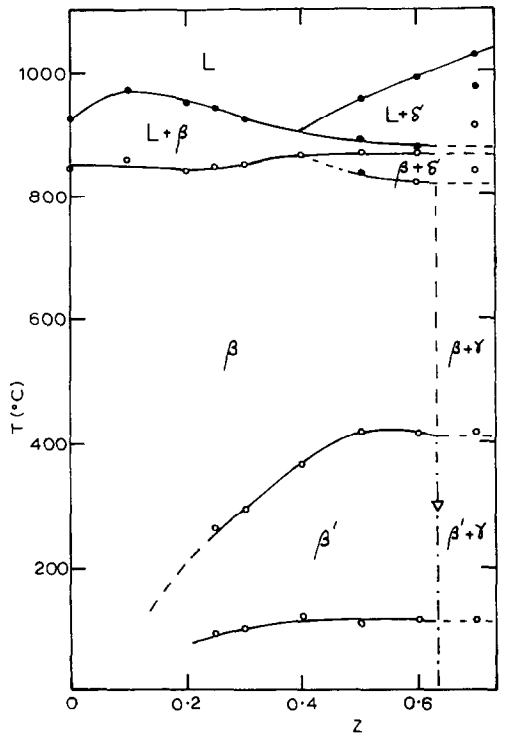

FIG. 5. $T(z)$ diagram for the $x = y$ section. β is the Mn-disordered zinc blende, β' the Mn-ordered zinc blende, γ and δ the NiAs and NaCl structures of MnTe, respectively. ○, heating run; ●, cooling run; ▽, from X-ray data.

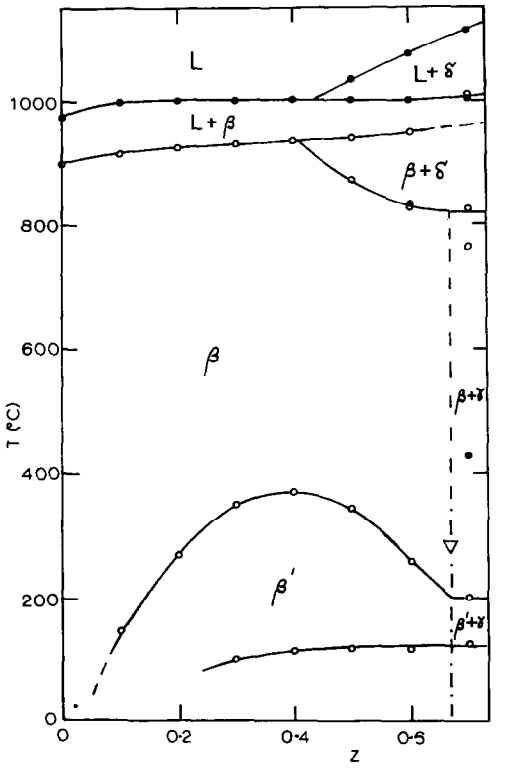

FIG. 6. $T(z)$ diagram for the $x = 3y$ section. β is the Mn-disordered zinc blende, β' the Mn-ordered zinc blende, and γ and δ are the NiAs and NaCl structures of MnTe, respectively. ○, heating run; ●, cooling run; ▽, from X-ray data.

(oc), β the Mn-disordered zinc blende (dzb), and β' the Mn-ordered zinc blende (ozb) forms. However, in the previous $T(z)$ diagram, the limit of the oc phases α' was shown as $z = 0.35$, but later measurements of magnetic susceptibility (*18*) and optical energy gap (*19*) showed that the α' could be present to the limits of solid solubility in the adamantine phases. Reexamination of the DTA data showed the presence at temperatures in the range 100–200°C of small peaks corresponding to the α'–β' transition. This modified boundary is shown in Fig. 3. In addition, a further transition was observed for $z > 0.2$ at temperatures of the order 100°C, and the resulting line is also shown in Fig. 3. At present, there are no data to indicate the phase conditions below this boundary.

The form of the boundary between the chalcopyrite and zinc blende phases, being an (α + β) two-phase field for $z < 0.20$ and a single line for $z > 0.20$, has been attributed to the ordering of the Mn atoms (*6*), the change at $z = 0.20$ corresponding to the point where the α–α' boundary meets the $\alpha(\alpha')$–β transition. Very similar results to those described above for the $x = 0$ section have been observed for the $(AgIn)_{1-z}Mn_{2z}Te_2$ diagram (*19*).

The behavior of the section $y = 3x$ (Fig. 4) in this lower temperature range is similar

to that of the $x = 0$ section. Again, α, α', β, and β' fields occur and, at temperatures below 200°C, the oc α' phase extends to the limit of solid solubility at $z = 0.60$. Also, at temperatures around 100°C, the boundary corresponding to the unknown transition mentioned above is again observed. In the cases of the $x = y$ and $x = 3y$ sections (Figs. 5 and 6), no chalcopyrite phase occurs but there is a wide range of solid solubility in the zinc blende structure, to $z = 0.65$ for $x = y$ and to $z = 0.72$ for $x = 3y$. For both of these sections, the boundary corresponding to the unknown transition is observed at approximately 100°C, as is shown in Figs. 5 and 6. Thus this transition is not limited to the chalcopyrite phase, but occurs for the ordered form of both of the adamantine structures.

At temperatures above the limit of the β field, the diagrams are more complicated and the designation of the phases in the various fields has been guided by the work of Aresti et al. (*5*). At the higher values of z, two-phase fields involving a phase δ occur, and this has been identified (*5*) as the rock-salt structure shown by MnTe above 1050°C, but which exists at lower temperatures elsewhere in the general diagram. It is clear that, in general, none of the sections shown are pseudo-binary in character. However, for the $x = 0$ section and for temperatures below 600°C, pseudo-binary conditions appear to be satisfied to a good approximation.

Conclusions

The DTA and X-ray results for the $Cd_{2x}(CuIn)_yMn_{2z}Te_2$ alloys show that a wide range of solid–solution occurs for both the chalcopyrite and zinc blende structures, and that for both structures an ordered form, attributed to the Mn ions ordering on the cation sublattice, occurs below approximately 550°C for values of $z < 0.5$.

Acknowledgments

The authors are grateful to Mr. F. Sánchez for technical assistance. They also thank Consejo de Desarrollo Científico Humanístico y Tecnológico (CDCHT), Universidad de Los Andes (ULA), and Consejo Nacional de Investigaciones Científicas y Tecnológicas (CONICIT) Venezuela for financial support.

References

1. J. A. Gaj, *J. Phys. Soc. Japan* **49,** 797 (1980).
2. J. K. Furdyna and J. Kossut (Eds.), "Semiconductors & Semimetals," Vol. 25, Academic Press, San Diego (1988).
3. M. Quintero, L. Dierker, and J. C. Woolley, *J. Solid State Chem.* **63,** 110 (1986).
4. M. Quintero and J. C. Woolley, *Phys. Status Solidi A* **92,** 449 (1985).
5. A. Aresti, L. Garbato, A. Geddo-Lehmann, and P. Manca, "Proceedings of the 7th International Conference on Ternary and Multinary Compounds," p. 497, Materials Research Society (1986).
6. M. Quintero, P. Grima, R. Tovar, G. S. Perez, and J. C. Woolley, *Phys. Status Solidi A* **107,** 205 (1988).
7. M. Quintero, R. Tovar, M. Al-Najjar, G. Lamarche, and J. C. Woolley, *J. Solid State Chem.* **75,** 136 (1988).
8. J. C. Woolley, G. Lamarche, A. Manoogian, M. Quintero, L. Dierker, M. Al-Najjar, D. Proulx, C. Neal, and R. Goudreault, "Proceedings of the 7th International Conference on Ternary and Multinary Compounds, p. 479, Materials Research Society (1986).
9. M. Quintero, P. Grima, J. E. Avon, G. Lamarche, and J. C. Woolley, *Phys. Status Solidi A* **108,** 599 (1988).
10. M. Quintero, P. Grima, R. Tovar, R. Gaudreault, D. Bissonnette, G. Lamarche, and J. C. Woolley, *J. Solid State Chem.* **76,** 210 (1988).
11. R. Chen and Y. Kirsh, "Analysis of Thermally Stimulated Processes, Int. Series of Sci. State," Vol. 15, p. 97, Pergamon, New York (1981).
12. E. Guerrero, M. Quintero, and J. C. Woolley, *J. Crystal Growth* **92,** 150–154 (1988).
13. E. Guerrero, M. Quintero, and J. C. Woolley, *J. Appl. Phys.* **63,** 2252 (1988).
14. R. Tovar, M. Quintero, C. Neal, and J. C. Woolley, *J. Cryst. Growth,* in press.
15. C. Neal, J. C. Woolley, R. Tovar, and M. Quintero, *J. Phys. D: Appl. Phys.* **22,** 1347 (1989).

16. R. TRIBOULET AND G. DIDIER, *J. Cryst. Growth* **52,** 614 (1981).
17. L. S. PALATNIK AND E. I. ROGACHEVA, *Sov. Phys. Dokl.* **12,** 503 (1967).
18. G. LAMARCHE, J. C. WOOLLEY, R. TOVAR, M. QUINTERO, AND V. SAGREDO, *J. Magn. Magn. Mater.* **80,** 321 (1989).
19. M. QUINTERO, R. TOVAR, M. DHESI, AND J. C. WOOLLEY, *Phys. Status Solidi A* **115,** 157 (1989).